Open access • Journal Article • DOI:10.1051/MECA/2017021

Numerical study of natural and mixed convection in a square cavity filled by a Cu–water nanofluid with circular heating and cooling cylinders — Source link

Zoubair Boulahia, Abderrahim Wakif, Ali J. Chamkha, Rachid Sehaqui

Institutions: University of Hassan II Casablanca, Prince Mohammad bin Fahd University

Published on: 01 Jan 2017 - Mechanics & Industry (EDP Sciences)

Topics: Natural convection, Combined forced and natural convection, Rayleigh number, Heat transfer and Grashof number

Mechanics & Industry **18**, 502 (2017)
© AFM, EDP Sciences 2017
DOI: 10.1051/meca/2017021

Mechanics & Industry

Available online at:
www.mechanics-industry.org

Regular Article

Numerical study of natural and mixed convection in a square cavity filled by a Cu–water nanofluid with circular heating and cooling cylinders

Zoubair Boulahia[1,*], Abderrahim Wakif[1], Ali J. Chamkha[2,3], and Rachid Sehaqui[1]

[1] Hassan II University, Faculty of Sciences Aïn Chock, Laboratory of Mechanics, BP 5366 Maarif, Casablanca, Morocco
[2] Mechanical Engineering Department, Prince Mohammad Bin Fahd University, Al-Khobar 31952, Saudi Arabia
[3] Prince Sultan Endowment for Energy and Environment, Prince Mohammad Bin Fahd University, Al-Khobar 31952, Saudi Arabia

Received: 14 September 2016 / Accepted: 9 May 2017

Abstract. The present study investigates the role of natural and mixed convection heat transfer of a Cu–water nanofluid in a square cavity with inside circular heating and cooling bodies. The finite volume discretization method with the Semi-Implicit Method for Pressure Linked Equations algorithm is employed for solving the two-dimensional Navier–Stokes and energy equations. The effects of various design parameters on the heat transfer rate are investigated. Design parameters used in this numerical simulation are the position and size of circular bodies. A wide range of parameters such as the Rayleigh number ($10^3 \leq Ra \leq 10^6$), volume fraction ($0 \leq \varphi \leq 0.05$), Richardson number ($0.01 \leq Ri \leq 1000$), and the Grashof number ($10^2 \leq Gr \leq 10^4$) has been used. The numerical analysis is carried out for the circular body's positions on the vertical centerline of the cavity. The circular body's positions on the vertical left-line of the cavity are also presented and discussed for comparison purposes. The results show that the optimal heat transfer is obtained when placing the circular body near the bottom wall. Furthermore, the effects of pair of circular bodies on the heat transfer rate are investigated. The simulations show that the heat transfer rate increases with changing the orientation of the pair of circular bodies from the horizontal to the vertical directions. For the case of the mixed convection process, it is found that at high Richardson numbers, the effect of moving walls decreases and the heat transfer rate changes significantly.

Keywords: circular body / natural convection / mixed convection / nanofluid

1 Introduction

Natural and mixed convection fluid flow and heat transfer is very important phenomenon for various engineering applications, such as heating and cooling nuclear systems of reactors, lubrication technologies, cooling of electronic devices, ventilation of rooms with radiators, cooling of containers and heat exchangers [1]. Therefore, enhancement of heat transfers in the cavities in several applications needs to add some cooling and/or heating bodies inside. Numerous investigations have been found on the natural convection (NC) [2,7] and mixed convection (MC) heat transfer in cavities filled with nanofluids [8,10]. The work of Khanafer and Aithal [8] was concentrated on the effect of MC flow and heat transfer characteristics in a lid-driven cavity with a circular body inside. The results showed that the average Nusselt number increases with an increase in the radius of the cylinder for various Richardson numbers and the optimal heat transfer results are obtained when placing the cylinder near the bottom wall. Islam et al. [9] investigated a numerical study on a lid-driven cavity with a heated square blockage. They found that size, location and Richardson number of the heater eccentricities affect the average Nusselt number of heater. Garoosi et al. [10] studied natural and MC heat transfer of nanofluid. Their simulations indicate that there is an optimum volume fraction of nanoparticles, where the maximum heat transfer occurs, and for MC by increasing Grashof number and decreasing Richardson number, the heat transfer rate increases. Deng [11] investigated laminar NC in a square cavity due to two and three discrete heat source–sink pairs on the vertical side walls. They observed that the heat transfer between walls of coolers and heaters is one-to one in a reversed manner. Oztop and Dagtekin [12] performed a numerical simulation on a square cavity with two moving walls. The obtained results show that when the vertical

* e-mail: boulahia.zoubair@gmail.com, zoubair.boulahia08@etude.univcasa.ma

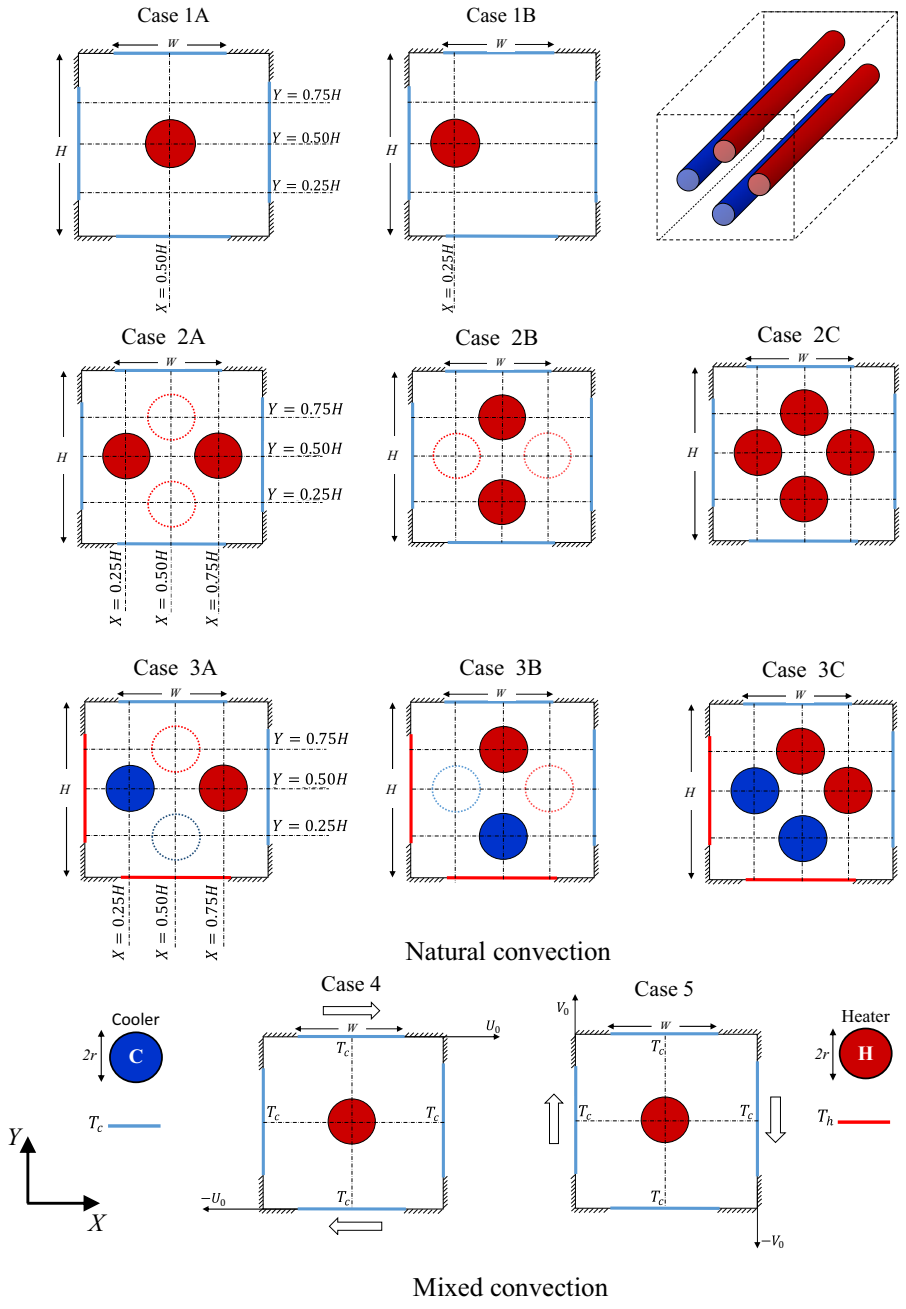

Fig. 1. Schematic of the cavity with circular bodies. Location of the circular bodies for each case is shown by dashed line.

walls move upwards in the same direction the heat transfer decreases significantly compared to when the vertical walls move in opposite directions. Talebi et al. [13] reported MC of nanofluids inside a differentially heated cavity (DHC) to note a direct relationship between the Rayleigh number and solid concentration.

Oztop et al. [14] reported a numerical simulation on a square cavity with two vertical adiabatic walls and two horizontal isothermal cold walls with a plate heater inside the cavity. Horizontal and vertical orientations of the heater were studied and the results showed that the heat transfer is higher in the case of vertical orientation of the heater compare to the horizontal orientation. Garoosi et al. [2] studied NC of nanofluids in a square cavity with several pairs of heaters and coolers (HAC). They found that the maximum and the minimum of heat transfer rate observed when the heater positioned at bottom and at top of cavity, they also found that the increasing size of the HAC and the Rayleigh number enhanced the heat transfer rate. Change of orientation from vertical to horizontal decreased the heat transfer, the effect of increasing number of HAC enhanced the heat transfer until a saturated number of HACs, and copper (Cu) produced slightly higher rate of heat transfer compare to TiO_2. Ho et al. [4,5] investigated experimentally and numerically the effects of the HAC position in an air filled circular enclosure with

Table 1. Thermo-physical properties of water and nanoparticles at $T = 300$ K [34].

	C_p (J kg^{-1} K)	ϱ (kg m^{-3})	K (W mK^{-1})	$\beta \times 10^5$ (K^{-1})	$\mu \times 10^6$ (kg m^{-1} s^{-1})	d_p (nm)
Copper (Cu)	385	8933	401	1.67	–	25
Water (H_2O)	4179	997.1	0.613	27.6	855	0.385

Table 2. Effect of the grid size on $\overline{Nu}_{tot}$ for case 1A and case 4 of Figure 1. The cavity filled with the Cu–water nanofluid ($\varphi = 0.05$) .

	63 × 63	83 × 83	103 × 103	123 × 123
Ra	Natural convection (case 1A) $R = 0.1$			
10^4	6.511	6.789	6.821	6.823
10^6	18.247	18.412	18.439	18.441
$Ri\,(Gr = 10^2)$	Mixed convection (case 4) $R = 0.15$			
0.1	11.669	11.750	11.794	11.802
10^3	9.014	9.148	9.213	9.217

Table 3. Comparison of $\overline{Nu}$ between the present results and those reported in the literature for a DHC at different Rayleigh numbers.

Ra	10^3	10^4	10^5	10^6
de Vahl Davis [32]	1.118	2.243	4.519	8.799
Relative error (%)	0.17	0.13	0.75	0.54
Barakos and Mitsoulis [33]	1.114	2.245	4.510	8.806
Relative error (%)	0.17	0.22	0.55	0.62
Dixit and Babu [3]	1.118	2.256	4.519	8.817
Relative error (%)	0.17	0.71	0.75	0.75
Present study	**1.116**	**2.240**	**4.485**	**8.751**
Grid size	83^2	83^2	83^2	103^2

insulated walls [4] and subjected to external convection [5] in the range of Rayleigh numbers between 10^4 and 10^7. They considered cases where the heater was positioned higher than the cooler and found that by increasing the gap between the HAC, the rate of heat transfer decreases. Park et al. [1] studied a numerical study on a square cavity with a pair of hot horizontal cylinders positioned at different vertical locations. They observed that the local Nusselt numbers on the surface of the cylinders strongly depend on the gap distance between the two hot cylinders and the walls of the cavity.

El Abdallaoui et al. [7] performed a numerical simulation of NC between a decentered triangular heating cylinder and centered triangular heating cylinder [15] in a square outer cylinder filled with a pure fluid or a nanofluid using the lattice Boltzmann method. The results indicated that the horizontal displacement from the centered position to decentered position led to a considerable increase of heat transfer at a weak Rayleigh number and the vertical displacement had the most important effect on heat transfer at high values of the Rayleigh number. Kalteh et al. [16] considered laminar MC of nanofluid in a

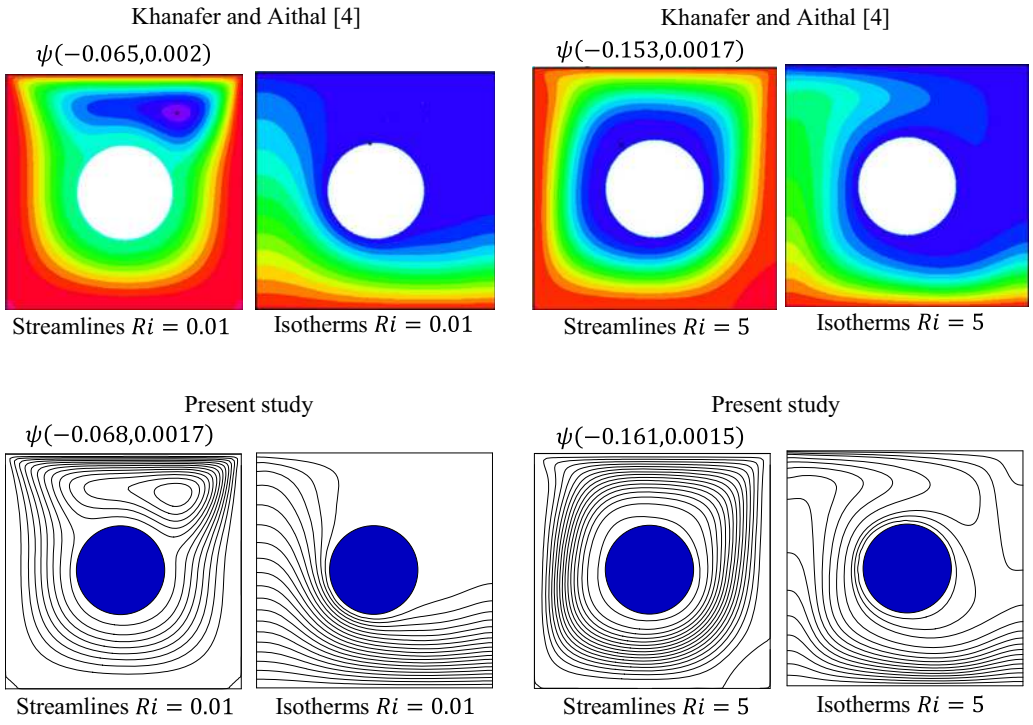

Fig. 2. Comparison of present results with the numerical results of Khanafer and Aithal [8] ($Re = 100$, $Pr = 0.7$, $r/H = 0.2$).

Table 4. Comparison of the average Nusselt number at the bottom wall of a lid driven cavity with an isothermal circular cylinder (T_c) between the present results and that of Khanafer and Aithal [8] ($Re = 100$, $Pr = 0.7$, $r/H = 0.2$).

$(\delta_x,\ \delta_y)$	$Ri = 0.01$			$Ri = 5$		
	Present	Khanafer and Aithal [8]	%Relative error	Present	Khanafer and Aithal [8]	%Relative error
(0.5, 0.7)	**2.24**	2.26	0.89	**2.86**	2.89	1.04
(0.5, 0.5)	**2.89**	2.92	1.03	**4.64**	4.70	0.64
(0.5, 0.3)	**5.18**	5.19	0.19	**5.53**	5.52	0.18

lid-driven square cavity with a triangular heat source. Their simulations indicated that increasing the volume fraction, the nanoparticles diameter and Reynolds number led to an increase in the average Nusselt number. Boulahia et al. [17] reported a MC of the nanofluids in two-sided lid-driven square cavity with a pair of triangular heating cylinders. They found that by reducing the diameter of the nanoparticles and Richardson number, the heat transfer rate increases, and by changing horizontal direction of the moving walls the heat transfer rate variation is negligible. Other examples can be found in references [18–21]. The work of AlAmiri et al. [22] addressed buoyancy-induced heat transfer in a partially divided square enclosure. Their investigations showed that increasing the height and width of the heater enhances the heat transfer owing to the increase in the surface area of the heater.

Brinkman [23] and Maxwell-Garnetts [24] are very basic models of viscosity and conductivity literately used in many applications of nanofluids, such as free convection of nanofluids [7,15] and MC of nanofluids [13] which take into consideration only the influences of volume fraction of nanoparticles for estimating the effective viscosity and thermal conductivity of the nanofluid. Various examinations show that conflicting results on the effects of nanofluid on the heat transfer rate in the enclosures can be obtained by using different models for estimating effective viscosity and conductivity of the nanofluid [25,26]. Experimental investigations propose that various parameters such as diameter, type of the nanoparticles and volume fraction and temperature of the nanofluid can significantly influence the thermal conductivity and effective viscosity of the nanofluid [27,28]. The new models indicate that enhancement in the rate of heat transfer is not similar with is predicted by simple models and in some cases increasing volume fraction of nanoparticles can even reduce the heat transfer rate [2].

The preceding researches indicate that the position, size and orientation of heat transfer bodies change the performance of heat transfer and changing properties of heat transfer fluid can also affect the performance of heat transfer mechanism. Recently, nanofluids, which are a

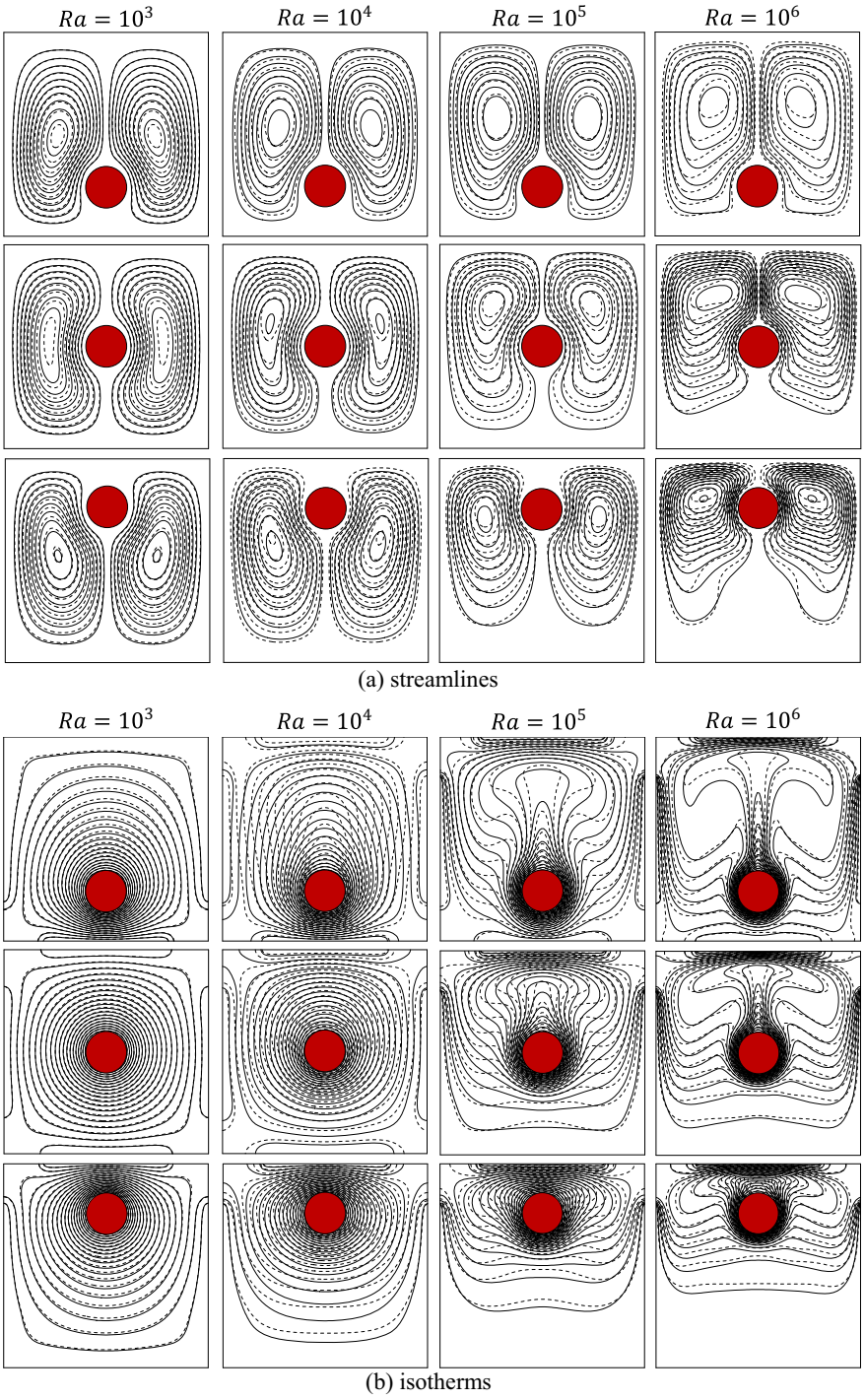

Fig. 3. (a) The streamlines and (b) isotherms inside the cavity corresponding to the position of the circular heating body ($R = r/H = 0.1$) on the VC of the cavity with case of pure fluid (dashed line) and Cu–water (solid line) nanofluid with $\varphi = 0.05$.

mixture of nanoparticles in a base fluid, with higher conductivity, are used to enhance the rate of heat transfer in many engineering applications.

In the present study, the main aim is to examine the free and MC heat transfer of nanofluid in a square enclosure with circular heating or cooling bodies. The first case under investigation characterizes the numerical models used in our study. The computational procedure elaborated in this study is validated against the numerical results of other investigations. In the other following sections, we study the effects of each design parameters which is simulated in the range of volume fraction between 0% and 5%. The new models of the thermal conductivity and effective viscosity investigated by Corcione et al. [25] are used to estimate thermophysical

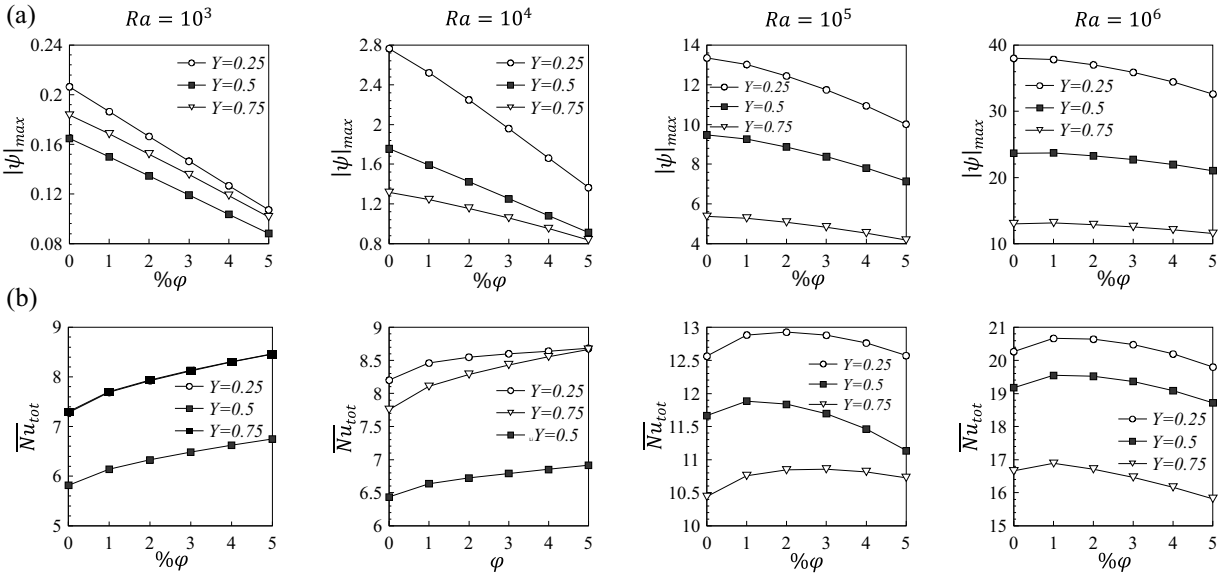

Fig. 4. Variation of (a) $\psi_{\max}$ and (b) $\overline{Nu}_{tot}$ in case of VC location for the three selected positions of the circular heating body at different Rayleigh numbers and volume fraction of the nanoparticles.

proprieties of the nanofluid. Our numerical results are presented in the form of plots of isotherms, streamlines and average Nusselt numbers to show the influence of nanofluid and design parameters.

2 Problem statement

The studied configurations and coordinate system of the considered enclosure in the present study are shown in Figure 1. The walls of the square enclosure are assumed to be partially cooled with isothermal partition $T_c = 290$ of a distance $w = 0.6$. The other parts of the enclosure are all thermally insulated. One circular heating body with constant temperature $T_h = 310$ is used inside the square cavity. Two cases are considered, i.e., case 1A where the heated body is symmetrically placed on the vertical centerline (VC) ($X = 0.5$) of the cavity, and case 1B where the heated body is placed on vertical left-line (VL) ($X = 0.25$) of the cavity. As shown in Figure 1, three cases are considered, i.e., case 2A where one pair of circular heating bodies is placed on the horizontal centerline (HC) of the cavity, case 2B where one pair of circular heating bodies is placed on the VC of the cavity, and case 2C where two pairs of circular heating bodies are used inside the cavity, one is placed on the VC of the cavity and the other on the HC.

Also, three other cases are considered, i.e., case 3A where one pair of circular heating and cooling bodies is placed on the HC of the cavity, case 3B where one pair of circular heating and cooling bodies is placed on the VC of the cavity, and case 3C where two pairs of circular heating and cooling bodies are used inside the cavity, one is placed on the VC of the cavity and the other on the HC. In addition, two cases are studied for MC, i.e., case 4 where the horizontal walls of the square cavity move in the opposite direction, and case 5 where the vertical walls of the square cavity move in the opposite direction. The thermo-physical properties of the nanofluid used in this study are evaluated at the average fluid temperature $(T_c + T_h)/2$ as listed in Table 1.

3 Mathematical formulation

The governing equations including the two-dimensional transient equations of the continuity, momentum and energy for an incompressible flow are expressed in the following format:

$$\frac{\partial u}{\partial x} + \frac{\partial v}{\partial y} = 0 \tag{1}$$

$$\frac{\partial u}{\partial t} + u\frac{\partial u}{\partial x} + v\frac{\partial u}{\partial y} = -\frac{1}{\rho_{nf}}\frac{\partial p}{\partial x} + \frac{\mu_{nf}}{\rho_{nf}}\left(\frac{\partial^2 u}{\partial x^2} + \frac{\partial^2 u}{\partial y^2}\right) \tag{2}$$

$$\frac{\partial v}{\partial t} + u\frac{\partial v}{\partial x} + v\frac{\partial v}{\partial y} = -\frac{1}{\rho_{nf}}\frac{\partial p}{\partial y} + \frac{\mu_{nf}}{\rho_{nf}}\left(\frac{\partial^2 v}{\partial x^2} + \frac{\partial^2 v}{\partial y^2}\right) + \frac{(\rho\beta)_{nf}}{\rho_{nf}}(T - T_c) \tag{3}$$

$$\frac{\partial T}{\partial t} + u\frac{\partial T}{\partial x} + v\frac{\partial T}{\partial y} = \alpha_{nf}\left(\frac{\partial^2 T}{\partial x^2} + \frac{\partial^2 T}{\partial y^2}\right) \tag{4}$$

where the nanofluid effective density, heat capacity, thermal expansion coefficient and thermal diffusivity are calculated from the following equations [6,29]:

$$\rho_{nf} = (1 - \varphi)\rho_f + \varphi\rho_s \tag{5}$$

$$(\rho C_p)_{nf} = (1 - \varphi)(\rho C_p)_f + \varphi(\rho C_p)_s \tag{6}$$

$$\begin{array}{llll} u=0 & \text{or} & -U_0, & v=0, T=T_c \quad \text{or} \quad T_h \quad \text{on bottom wall of the cavity} \\ u=0 & \text{or} & U_0, & v=0, T=T_c \quad \text{on upper wall of the cavity} \\ v=0 & \text{or} & -V_0, & v=0, T=T_c \quad \text{on right wall of the cavity} \\ u=0 & \text{or} & V_0, & v=0, T=T_c \quad \text{or} \quad T_h \quad \text{on left wall of the cavity} \end{array} \tag{13}$$

$$\begin{array}{llll} U=0 & \text{or} & -1, & V=0, \theta=0 \quad \text{or} \quad 1 \quad \text{on bottom wall of the cavity} \\ U=0 & \text{or} & 1, & V=0, \theta=0 \quad \text{on upper wall of the cavity} \\ V=0 & \text{or} & -1, & V=0, \theta=0 \quad \text{on right wall of the cavity} \\ U=0 & \text{or} & 1, & V=0, \theta=0 \quad \text{or} \quad 1 \quad \text{on left wall of the cavity} \end{array} \tag{21}$$

$$(\rho\beta)_{nf} = (1-\varphi)(\rho\beta)_f + \varphi(\rho\beta)_s \tag{7}$$

$$\alpha_{nf} = k_{nf}/(\rho C_p)_{nf} \tag{8}$$

The Corcione model [6,25] for the dynamic viscosity and the thermal conductivity of the nanofluid are given by:

$$\mu_{nf} = \mu_f/(1-34.87(d_p/d_f)^{-0.3}\varphi^{1.03}) \tag{9}$$

$$\frac{k_{nf}}{k_f} = 1 + 4.4Re_B^{0.4}Pr^{0.66}\left(\frac{T}{T_{fr}}\right)^{10}\left(\frac{k_p}{k_f}\right)^{0.03}\varphi^{0.66} \tag{10}$$

$$Re_B = \frac{\rho_f u_B d_p}{\mu_f} \tag{11}$$

$$u_B = \frac{2k_bT}{\pi\mu_f d_p^2} \tag{12}$$

All terms are defined in the nomenclature.

The boundary conditions for NC and MC are written as:

see equation (13) above

The following dimensionless variables for NC and MC are defined based on properties of pure fluid:

$$\tau = \frac{t}{H/U_{ref}}, \quad X = \frac{x}{H}, \quad Y = \frac{y}{H}, \quad U = \frac{u}{U_{ref}}, \quad V = \frac{v}{U_{ref}}, \quad P = \frac{p}{\rho_{nf}U_{ref}^2}, \quad \theta = \frac{T-T_c}{T_h-T_c} \tag{14}$$

where U_{ref} is considered to be α_f/H and U_0 are for NC and MC, respectively. The dimensionless numbers for the system are defined as:

$$Re = \frac{u_{ref}H}{\nu_{nf}}, \quad Ri = \frac{Gr}{Re^2}, \quad Gr = \frac{g\beta_f(T_h-T_c)H^3}{\nu_f^2} \tag{15}$$

$$Ra = \frac{g\beta_f(T_h-T_c)H^3}{\alpha_f\nu_f}, \quad Pr = \frac{\nu_f}{\alpha_f} \tag{16}$$

The governing equations (1)–(4) are written in the following dimensionless form:

$$\frac{\partial U}{\partial X} + \frac{\partial V}{\partial Y} = 0 \tag{17}$$

$$\frac{\partial U}{\partial \tau} + U\frac{\partial U}{\partial X} + V\frac{\partial U}{\partial Y} = -\frac{\partial P}{\partial X} + C\frac{\rho_f}{\rho_{nf}}\frac{\mu_{nf}}{\mu_f}\left(\frac{\partial^2 U}{\partial X^2} + \frac{\partial^2 U}{\partial Y^2}\right) \tag{18}$$

$$\frac{\partial V}{\partial \tau} + U\frac{\partial V}{\partial X} + V\frac{\partial V}{\partial Y} = -\frac{\partial p}{\partial Y} + C\frac{\rho_f}{\rho_{nf}}\frac{\mu_{nf}}{\mu_f}\left(\frac{\partial^2 V}{\partial X^2} + \frac{\partial^2 V}{\partial Y^2}\right) + C'\frac{(\rho\beta)_{nf}}{\rho_{nf}\beta_f}\theta \tag{19}$$

$$\frac{\partial \theta}{\partial \tau} + U\frac{\partial \theta}{\partial X} + V\frac{\partial \theta}{\partial Y} = C''\frac{\alpha_{nf}}{\alpha_f}\left(\frac{\partial^2 \theta}{\partial X^2} + \frac{\partial^2 \theta}{\partial Y^2}\right) \tag{20}$$

where C, C', and C'' are given for case of NC or MC:

	C	C'	C''
Natural convection (NC)	Pr	$Ra \cdot Pr$	1
Mixed convection (MC)	$1/Re$	Ri	$1/(Pr \cdot Re)$

The dimensionless form of the boundary conditions for NC and MC can be written as:

see equation (21) above

The total mean Nusselt number of all cavity's walls is defined as:

$$\overline{Nu}_{tot} = \frac{1}{w}\int_{\frac{H}{2}-\frac{w}{2}}^{\frac{H}{2}+\frac{w}{2}}\frac{k_{nf}(\varphi)}{k_f}\left\{\left|\frac{\partial\theta}{\partial X}\right|_{left} + \left|\frac{\partial\theta}{\partial X}\right|_{right}\right\}dY + \frac{1}{w}\int_{\frac{H}{2}-\frac{w}{2}}^{\frac{H}{2}+\frac{w}{2}}\frac{k_{nf}(\varphi)}{k_f}\left\{\left|\frac{\partial\theta}{\partial Y}\right|_{bottom} + \left|\frac{\partial\theta}{\partial Y}\right|_{upper}\right\}dX \tag{22}$$

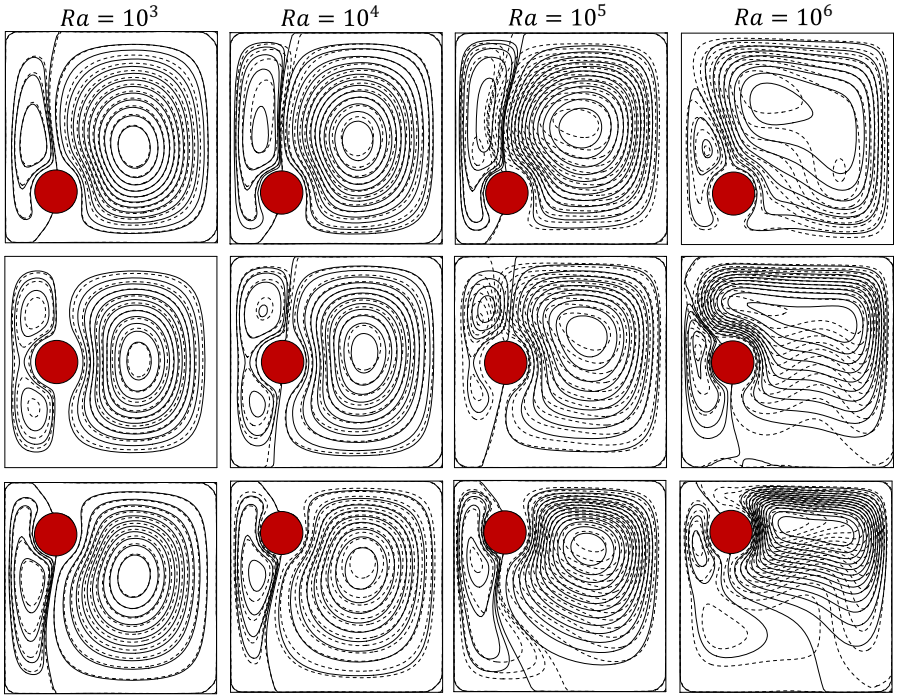

(a) streamlines

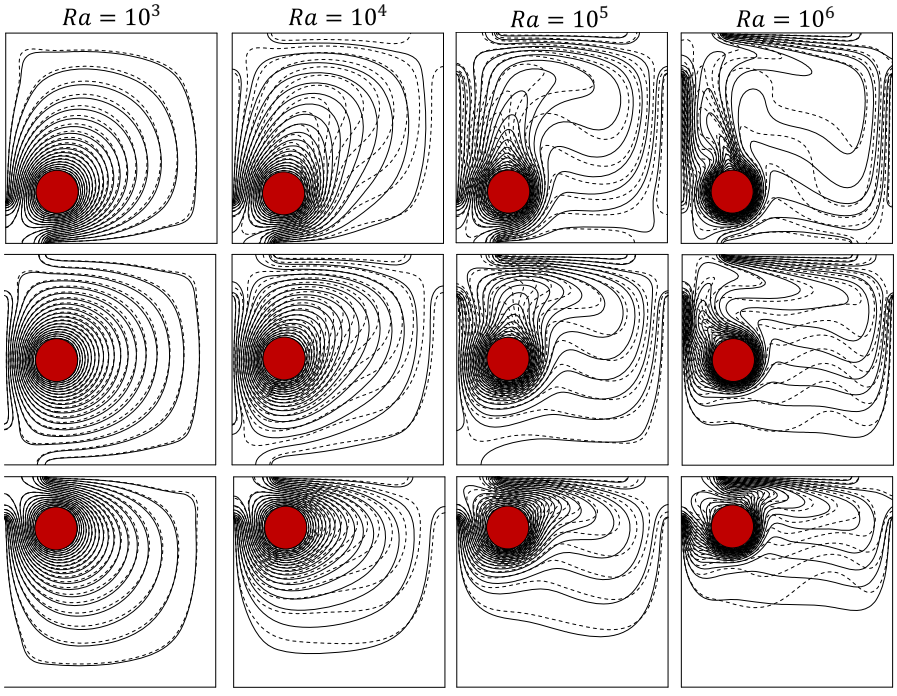

(b) isotherms

Fig. 5. (a) The streamlines and (b) isotherms inside the cavity corresponding to the position of the circular heating body ($R = r/H = 0.1$) on the VL of the cavity with case of pure fluid (dashed line) and Cu–water (solid line) nanofluid with $\varphi = 0.05$.

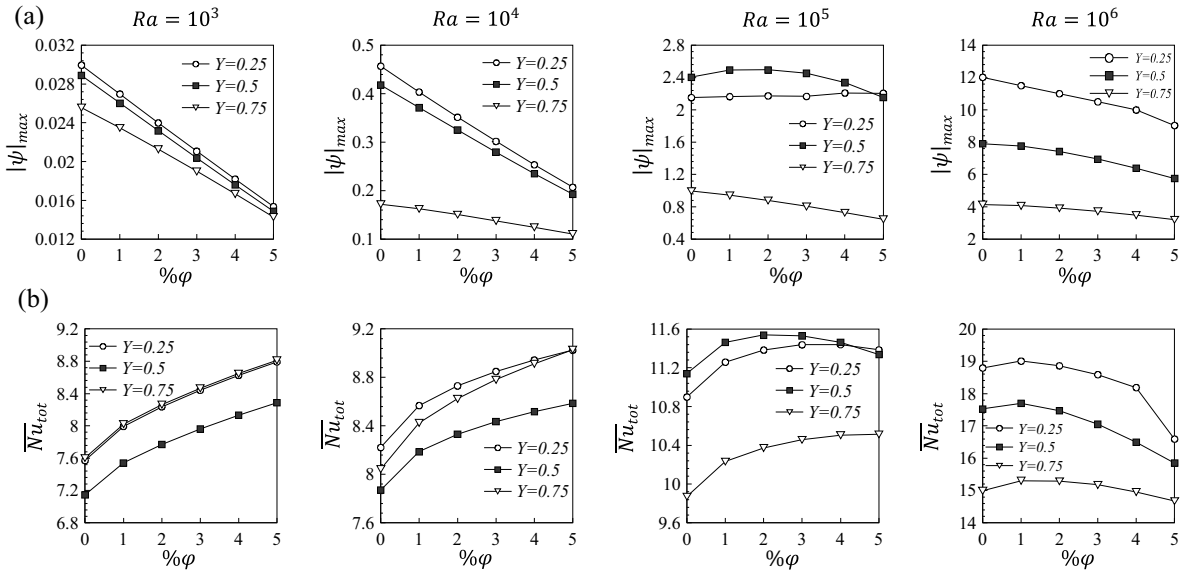

Fig. 6. Variation of (a) $\psi_{\max}$ and (b) $\overline{Nu}_{tot}$ in case of VL location for the three selected positions of the circular heating body at different Rayleigh numbers and volume fraction of the nanoparticles.

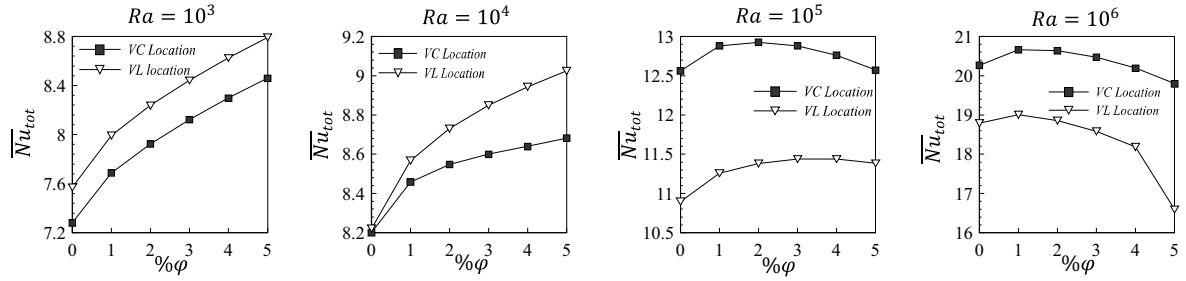

Fig. 7. Comparison of $\overline{Nu}_{tot}$ between VC and VL location of the circular heating body at different Rayleigh numbers and volume fraction of the nanoparticles with case of body is positioned at bottom.

4 Numerical details

The discretization procedure of the governing equations (Eqs. (17)–(20)) and boundary conditions described by equation (21) is based on a finite volume formulation, given by Patankar [30] on a staggered grid. The Semi-Implicit Method for Pressure Linked Equations procedure is used to solve the coupled pressure–velocity equation while hybrid differencing scheme of Spalding [31] is used for the convective terms. Line by line application of Tri-Diagonal Matrix Algorithm method [31] is applied on equation systems until sum of the residuals became less than 10^{-6}. The developed algorithm is implemented in FORTRAN program.

4.1 Grid independence study

In order to determine a proper grid for the numerical simulation, a square cavity filled with a Cu–water nanofluid ($\varphi = 0.05$) is analyzed in two extreme Rayleigh numbers ($Ra = 10^3$ and 10^6) and Richardson number ($Ri =$ 0.1 and 1000) for both NC and MC configurations. The mean Nusselt number obtained using different grid numbers for particular cases is presented in Table 2. As can be observed from the table, a non-uniform 103×103 grid is sufficiently fine for the numerical calculation.

4.2 Validations

The present numerical scheme is validated against various numerical results available in the literature, two different heat convection problems are chosen. The first case is the benchmark problem of NC in a square cavity which considered by De Vahl Davis [32] filled with air ($Pr = 0.71$). Table 3 demonstrates an excellent comparison of the average Nusselt number between the present results (bold values) and the numerical results found in the literature [3,32]. The second case is a MC flow and heat transfer characteristics in a lid-driven cavity with a circular body inside. Figure 2 illustrates a comparison of the isotherms and streamlines between the present results and the results reported by Khanafer and Aithal [8] at a Reynolds number ($Re = 100$) for various Richardson numbers. The results shown in Table 4 (bold values) provide sufficient confidence in the present numerical scheme.

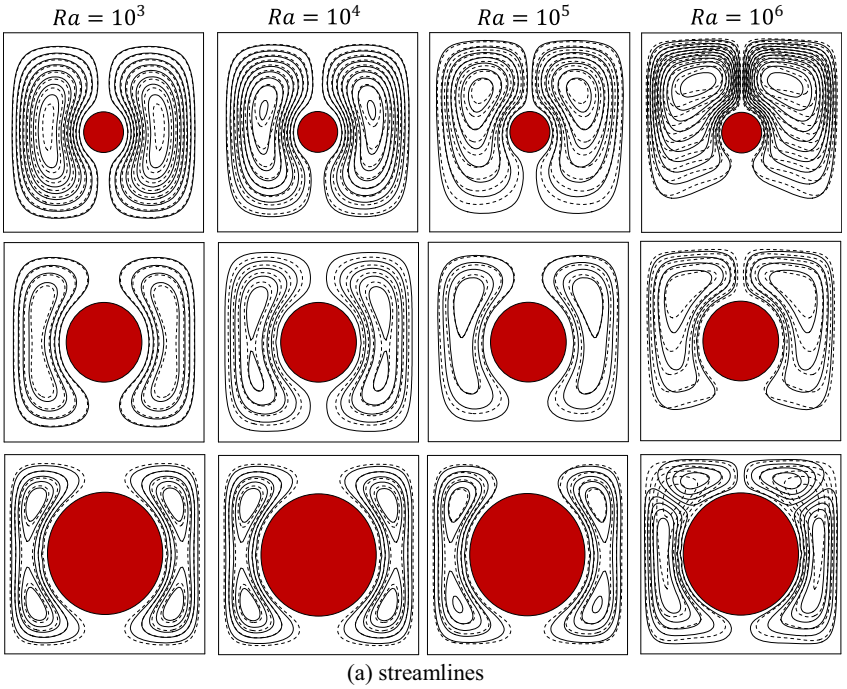

(a) streamlines

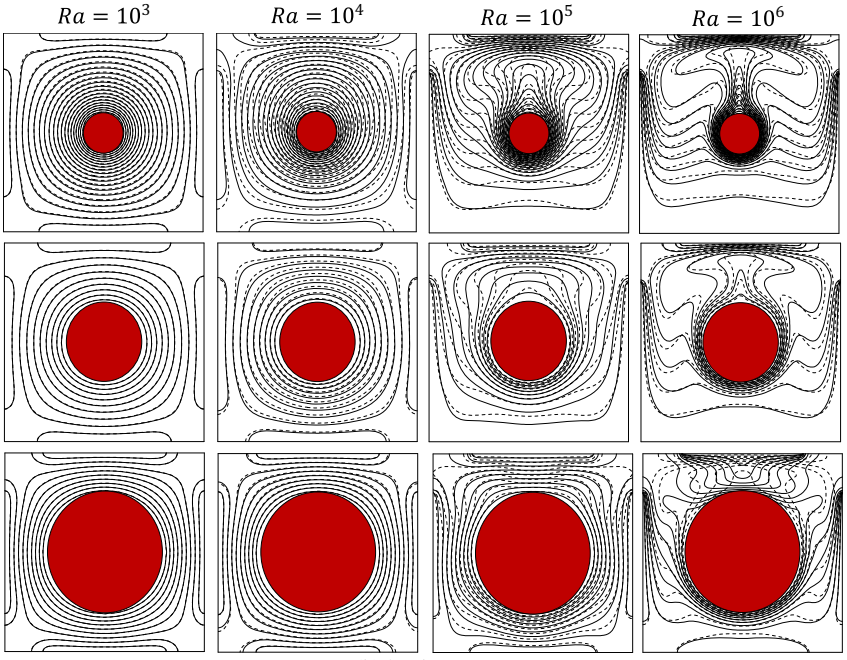

(b) isotherms

Fig. 8. (a) The streamlines and (b) isotherms inside the cavity corresponding to different sizes of circular heating body, i.e., $R = r/H = 0.1$, 0.2 and 0.3 with case of pure fluid (dashed line) and Cu–water (solid line) nanofluid with $\varphi = 0.05$.

5 Results and discussion

In the present study, direct simulations with the finite volume method are carried out for natural and MC heat transfer of a nanofluid (Cu–water) in a square cavity with inside circular heating and cooling bodies. The key parameters used in this numerical simulation are: the position and size of circular bodies. Wide range of parameters such as the Rayleigh number ($10^3 \leq Ra \leq 10^6$), volume fraction $0 \leq \varphi \leq 0.05$, Richardson number ($0.01 \leq Ri \leq 1000$), Grashof number $10^2 \leq Gr \leq 10^4$, position of circular heating body ($0.25 \leq Y \leq 0.75$) and the radius of the circular body ($0.1 \leq R \leq 0.3$) have been used. The results are presented in separate sections.

5.1 NC configuration

5.1.1 Position of circular body

The streamlines and isotherms corresponding to the position of the circular heating body on the VC of the cavity are presented in Figure 3 for which the Rayleigh

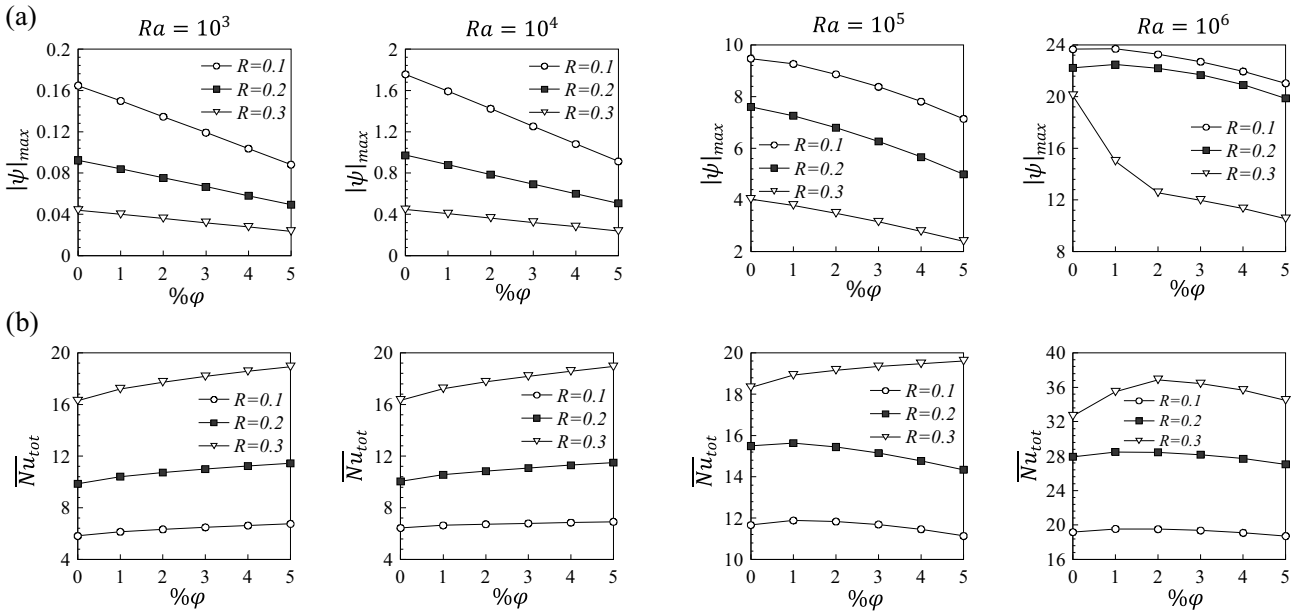

Fig. 9. Variation of (a) $\psi_{\max}$ and (b) $\overline{Nu}_{tot}$ corresponding to different sizes of circular heating body, i.e., $R = r/H = 0.1$, 0.2 and 0.3 at different Rayleigh numbers and volume fraction of the nanoparticles.

number is altered between 10^3 and 10^6. The circular heating body is fixed on the VC of the cavity and its position is changed from bottom to top ($Y = 0.25$, 0.5 and 0.75) at different Rayleigh numbers and volume fractions of nanoparticles. Figure 3 shows the effect of changing the position of the circular heating body on the streamlines and isotherms. The cavity is filled with a Cu–water nanofluid ($\varphi = 5\%$), for comparisons, the streamlines and the isotherms for pure fluid and nanofluid are shown by dashed line and solid line respectively, we can see in Figure 3(a) that the flow is symmetrical with respect to the VC of the cavity. The flow structure is organized into two convection cells, one clockwise vortex on the right and one counter-clockwise vortex on the left. For $Ra = 10^3$ and 10^4, the isotherms shown in Figure 3(b) are uniformly distributed which indicate that the heat transfer in the cavity is governed mainly by the conduction mode. When the circular heating body is positioned at the bottom, at the middle or at top, the bicellular symmetrical structure of the flow is still preserved. The centers of the convection cells are located below the circular body which is positioned at the top and the central vortex core changes significantly by changing the position of the body from the bottom to the top. By increasing the Rayleigh number from 10^3 to 10^5, 10^6 and hence the buoyancy force, the concentration of the isotherms in the vicinity of the circular heating body and at the top wall increases too. The form of the isotherms becomes more and more complex which means that the heat transfer mechanism is changing from conduction to the convection regime, the case illustrating a convection mode ($Ra = 10^5$, 10^6). Figure 3(a) indicates that the centers of the vortex core are considerably shifted upward and become close to the median vertical plane of the cavity in all cases of body position. At $Ra = 10^6$ when the circular body located at bottom ($Y = 0.25$) or at medium ($Y = 0.25$), we can see in Figure 3(b) a vertical stratification of temperature near to VC of the cavity like a plum where there is the hot fluid compare to the neighboring fluid.

Variation of the total averaged Nusselt number $\overline{Nu}_{tot}$ and the maximum stream function $\psi_{\max}$ for the three selected positions of the circular heating body at different Rayleigh numbers and volume fractions of nanoparticles are presented in Figure 4. The maximum stream function $\psi_{\max}$ shows in Figure 4(a) decreases at all Rayleigh numbers by increasing the volume fraction of nanoparticles, we can explain the decrease of $\psi_{\max}$ by equation (9) which indicates that increasing volume fraction of the nanoparticles leads to an increase in the viscosity of the fluid. Figure 4(b) shows that changing the position of the circular heating body has a significant effect on the heat transfer rate. When $Ra = 10^3$, we can see in Figure 4(b) that the values of $\overline{Nu}_{tot}$ are the same in the case of bottom and top body positions. By increasing the Rayleigh number from 10^3 to 10^5, 10^6, the buoyancy force becomes significantly important, the maximum and the minimum values of $\overline{Nu}_{tot}$ are observed when the circular heating body is positioned at the bottom and at the top of the cavity, respectively. At high values of the Rayleigh number, the optimum volume fraction of nanoparticles which maximizes the heat transfer rate in most cases is about 1% (Fig. 4(b)).

The case for which the circular body is positioned on the VL of the cavity is shown in Figure 5. We can see at small values of the Rayleigh number ($Ra = 10^3$, 10^4) in all cases of body position that the flow symmetry is destroyed and the horizontal displacement of the circular body from the VC to the VL of the cavity induces a big cell much more intense and a small cell less intense than the latter. It is worth mentioning that for $Ra = 10^3$ and 10^4 (case of dominating conduction) the isotherms shown in Figure 5(b) are uniformly distributed, but at high values of the Rayleigh number ($Ra = 10^5$, 10^6), the path of the fluid particles

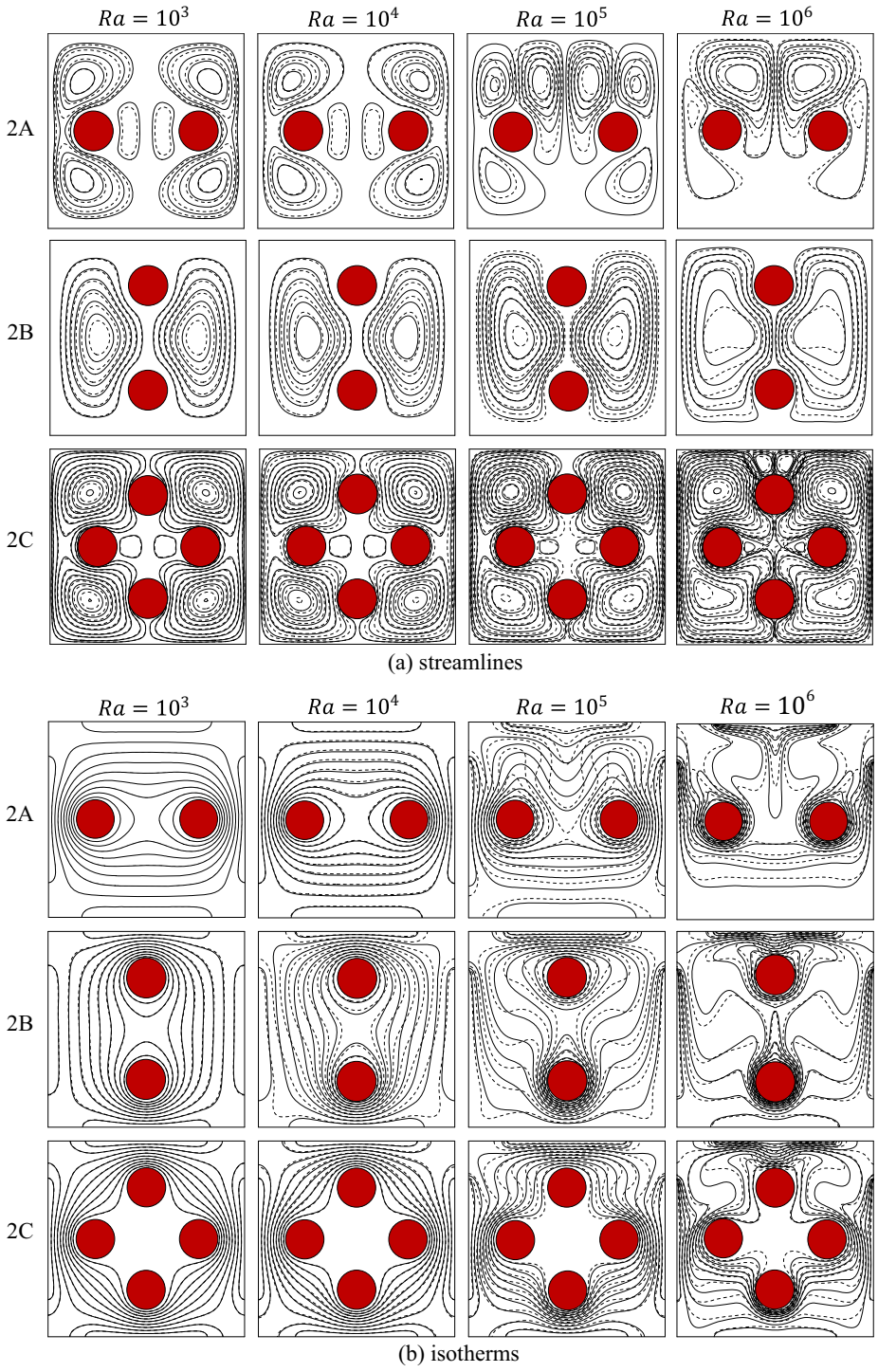

Fig. 10. (a) The streamlines and (b) isotherms inside the cavity for case 2A to 2C at different Rayleigh numbers with case of pure fluid (dashed line) and Cu–water (solid line) nanofluid with $\varphi = 0.05$.

becomes more and more complex which indicates that the main heat transfer mechanism is through convection. By increasing Ra beyond 10^5, it is observed in Figure 5(a) that the increase of the flow intensity in the upper part of the cavity overweighs its increase in its lower part, which shows that the centers of the big vortex are located above the circular body in the case where the body is positioned at the bottom or at the middle.

Figure 6 shows the variations of $\psi_{\max}$ and $\overline{Nu}_{tot}$ under the same conditions as shown in Figure 5. It is also observed in the case of the VL of the cavity that by increasing the volume fraction of nanoparticles, the value of $\psi_{\max}$ decreases. In addition, in Figure 6(a), by increasing Ra beyond 10^4, we can observe clearly that there is an optimum volume fraction of nanoparticles φ_{opt} for which the heat transfer rate is maximum. According to

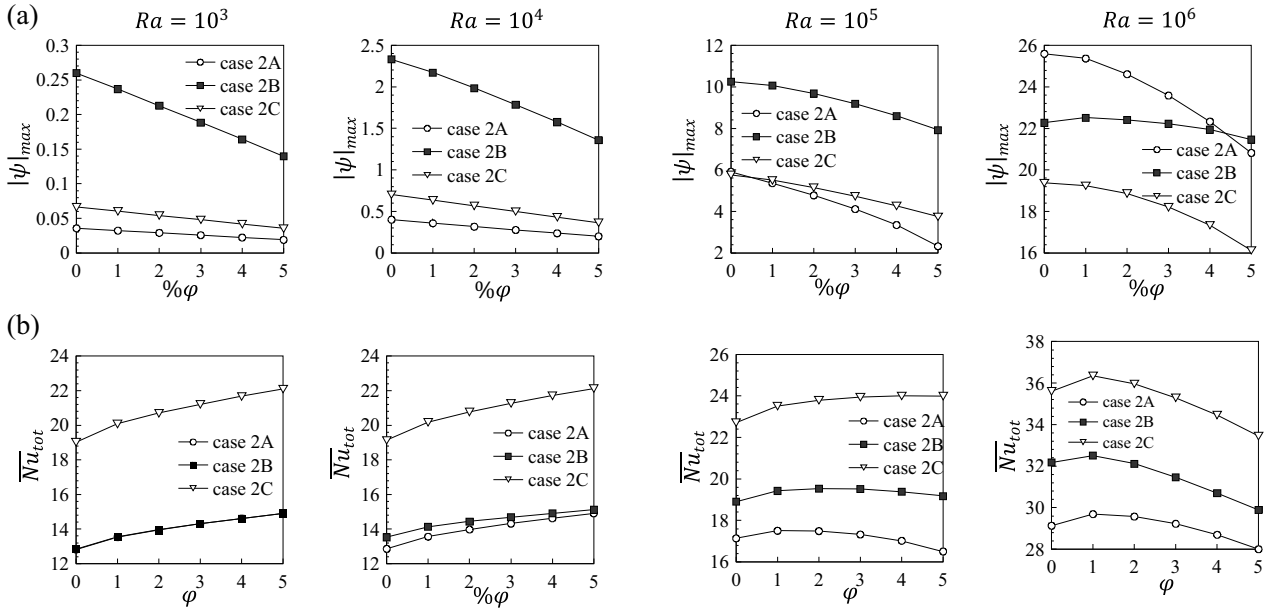

Fig. 11. Variation of (a) $\psi_{\max}$ and (b) $\overline{Nu}_{tot}$ for case 2A to 2C at different Rayleigh numbers and volume fraction of the nanoparticles.

equations (9) and (10), increasing the volume fraction of nanoparticles enhances the thermal conductivity but at $\varphi > \varphi_{opt}$, the adverse effects of the viscosity are more important than the positive effects of the thermal conductivity which leads to decrease the heat transfer rate. Similar remarks are also observed by Garoosi et al. [2]. At small values of the Rayleigh number ($Ra = 10^3$, 10^4), the effect of changing the circular body position from the bottom to the top is slightly negligible, as shown clearly in Figure 6(b), but when Ra exceeds ($Ra = 10^6$), we can observe an important difference in the heat transfer rate between the position of the body at the bottom and at the top. In Figure 6(b) at $Ra = 10^6$, it is also noticed that the maximum and the minimum values of $\overline{Nu}_{tot}$ are observed when the circular heating body is positioned at the bottom and at the top of the cavity, respectively.

The comparison concerning $\overline{Nu}_{tot}$ of the horizontal displacement of the circular heating body from the VC to the VL of the cavity in the case when the circular body is positioned at the bottom is shown in Figure 7. It is observed that at small Rayleigh numbers ($Ra = 10^3$, 10^4), the displacement of the circular heating body from the VC to the VL of the cavity leads to an increase in the heat transfer rate. At high values of the Rayleigh number ($Ra = 10^5, 10^6$), the enhancement of the heat transfer rate is observed when the circular body is positioned at the VC of the cavity, and this can be explained by the more space in the case of the VC of the cavity which results in a better circulation of the flow in the cavity and hence, improvements of the convection heat transfer (at high Ra).

From the preceding results in this section, we can conclude that the vertical displacement of the circular body has the most important effect on the heat transfer rate at high Rayleigh numbers and the horizontal displacement from the VC to the VL of the cavity increases the heat transfer at small Rayleigh numbers. Similar remarks were also reported by El Abdallaoui et al. [7].

5.1.2 Size of circular heating body

We present in this section three different sizes of the circular heating body, i.e., $R = r/H = 0.1$, 0.2 and 0.3, which are examined in a cavity filled with a Cu–water nanofluid with $\varphi = 0.05$. Figure 8 displays the effects of the circular body size on the streamlines and the isotherms for different values of the Rayleigh number. Figure 8(a) shows that at $Ra = 10^3$ and 10^4 (case of dominating conduction), two overall rotating symmetric eddies exist. By increasing the size of the circular heating body from $R = 0.1$ to 0.3, we can see clearly that the rotating symmetric eddies become with two inner vortices, respectively. At $Ra = 10^4$ for a size $R = 0.3$, the patterns of the isotherms (Fig. 8(b)) and the streamlines are about the same as those for $Ra = 10^3$. It is worth mentioning that at $Ra = 10^3$, 10^4 and 10^5, increasing the size of the circular heating body to $R = 0.3$, weakens the strength of the flow circulation and hence, the conduction becomes stronger and significantly dominant. By increasing the Rayleigh number up to 10^5 (and therefore, the buoyancy force), the role of convection in heat transfer becomes more significant. In Figure 8(b) for sizes $R = 0.1$ and 0.2, a plume starts to appear on the top of the circular heating body, and the presence of high-temperature gradients across this plume makes the upper part much more intense concerning the thermal gradient than the lower part. The flow at the bottom of the cavity is very weak compared with that at the top regions, which suggests stratification effects in the lower part of cavity. At $Ra = 10^6$, increasing the size R to 0.3 causes the rise of two secondary vortices, located in the upper surface of the circular heating body, while the primary eddies move to the side walls (see Fig. 8(a)).

Figure 9 shows the values of $\psi_{\max}$ and $\overline{Nu}_{tot}$ at different Rayleigh numbers and volume fractions of nanoparticles. By increasing the size of the circular body and the Rayleigh number, the heat transfer rate enhances.

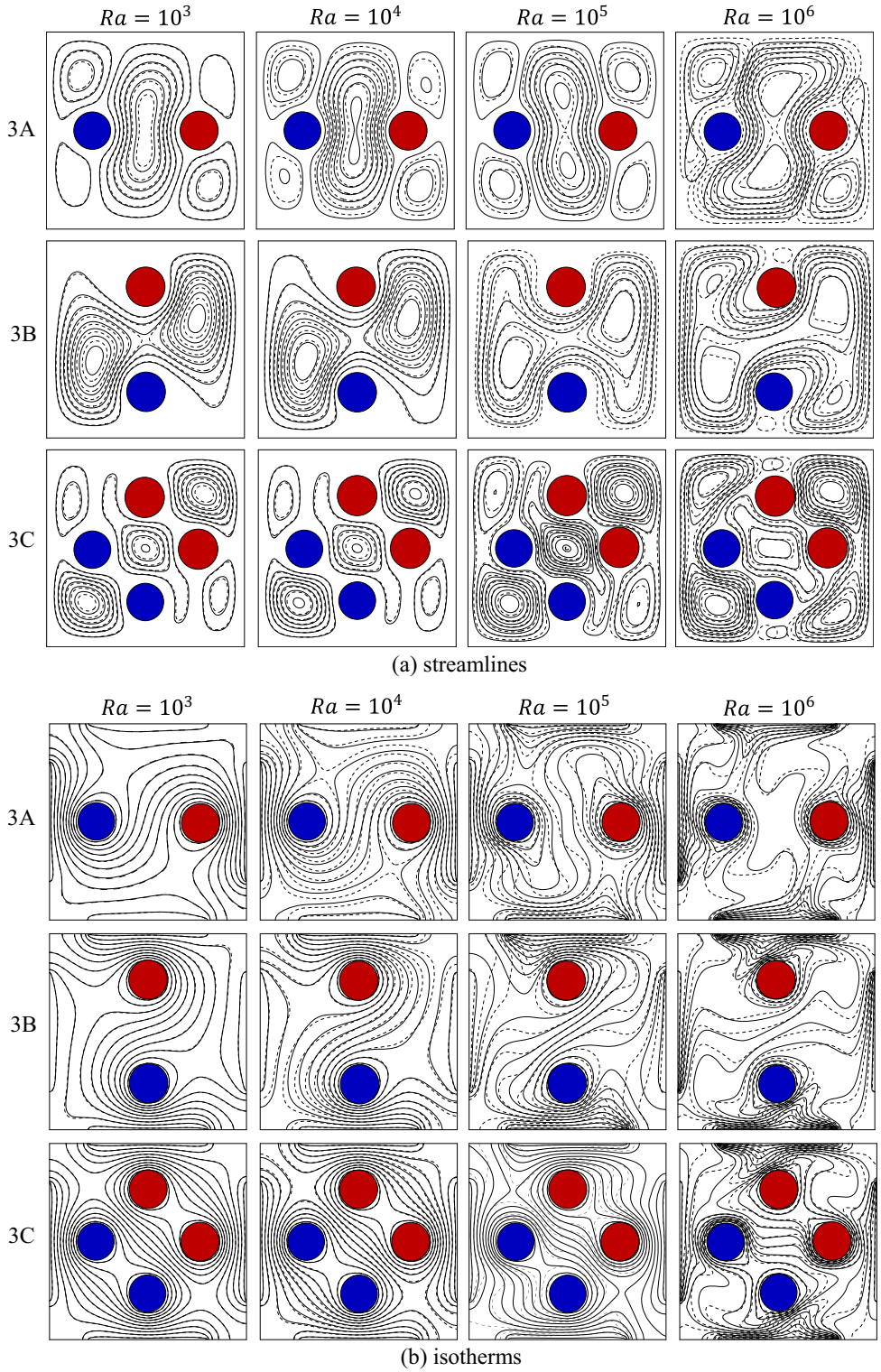

Fig. 12. The streamlines and (b) isotherms inside the cavity for case 3A to 3C at different Rayleigh numbers with case of pure fluid (dashed line) and Cu–water (solid line) nanofluid with $\varphi = 0.05$.

At small values of Rayleigh number ($Ra = 10^3$ and 10^4), we have seen that the conduction is significantly dominant at the biggest size of the circular heating body and therefore, enhancement of the heat transfer rate is maximum for $\varphi = 5\%$. At high Rayleigh numbers ($Ra = 10^5$ and 10^6), the optimum value of φ is about 1% in most cases.

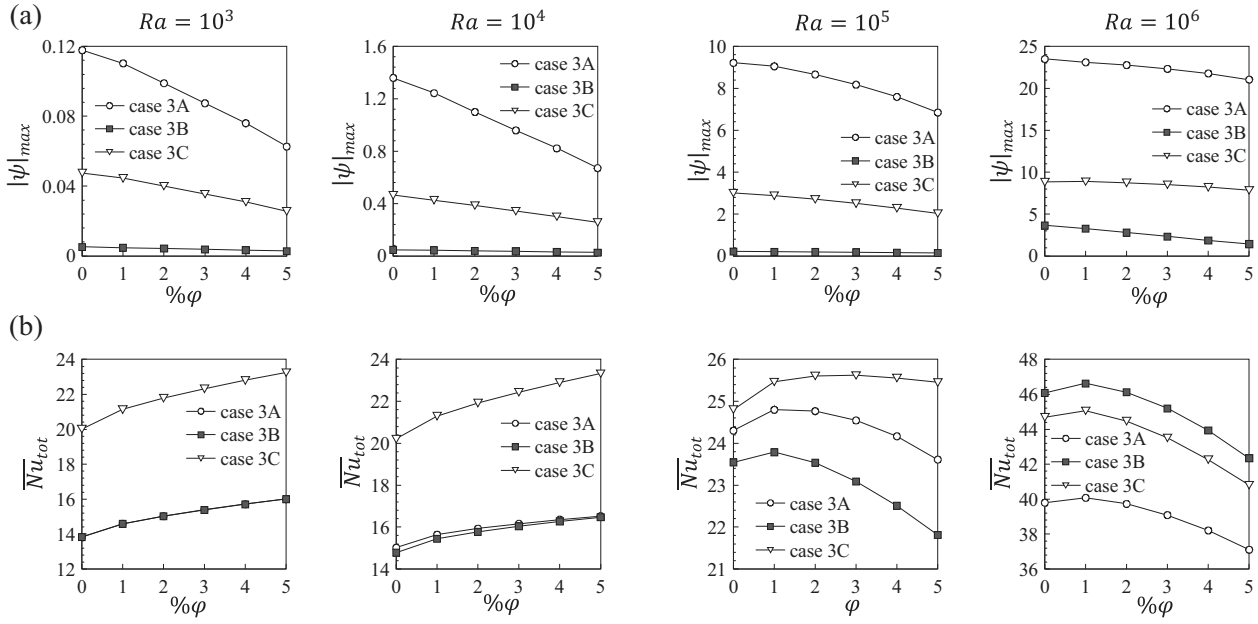

Fig. 13. Variation of (a) $\psi_{\max}$ and (b) $\overline{Nu}_{tot}$ for case 3A to 3C at different Rayleigh numbers and volume fraction of the nanoparticles.

5.1.3 Effect of one pair of circular heating bodies

In this section, results on the effect of one pair of circular heating bodies on the fluid flow and heat transfer rate are presented considering three different cases (2A, 2B and 2C) represented in Figure 1 which are explained in three steps.

Figure 10(2A) shows the effect of one pair of circular heating bodies which is placed at the HC of the cavity, on the streamlines and the isotherms at different Rayleigh numbers, defined in the first step. When $Ra = 10^3$, heat transfer in the cavity is governed mainly by the conduction mode. Thus, the streamlines and the isotherms are almost symmetric about the HC of the cavity, as shown in Figure 10(2A). The circulation of the flow shows two vortices appearing near each circular body, one in the upper side and the other in the lower side. At $Ra = 10^4$, the patterns of the isotherms and the streamlines are almost similar to those when $Ra = 10^3$, as shown in Figure 10(2A). At $Ra = 10^5$, the role of convection in heat transfer becomes more significant, for this reason we see clearly two secondary vortices appearing in the upper side between the pair of circular heating bodies, and hence, the intensity of flow in the lower side becomes less than that in the upper side. The thermal boundary layer around the surface of the two circular bodies becomes thinner, and the isotherms in the lower side are stratified which is a sign of a weak convection. However, the isotherms at the upper side become more tightened where the thermal plumes rising from the two circular body. By increasing Ra beyond 10^5 and hence, the buoyancy force, the intensity of the two vortices between the two circular bodies increases and the two secondary vortices become weakened. The thermal plumes on each circular body become much stronger than those of $Ra = 10^5$.

In the second step, the effects of one pair of circular heating bodies which is placed at the VC of the cavity, on the fluid flow and heat transfer rate are investigated at different Rayleigh numbers. The streamlines and the isotherms are shown in Figure 10(2B). The flow is symmetrical with respect to the VC of the cavity, and its structure is organized into two vortices, one clockwise vortex on the right and one counter-clockwise vortex on the left. At $Ra = 10^3$ and 10^4, the isotherms shown in Figure 10 (2B) are uniformly distributed which indicates that the heat transfer in the cavity is governed mainly by the conduction mode. When $Ra = 10^5$ and 10^6, the case illustrating a dominating convection regime, Figure 10 (2B) shows that the centers of the convection cells become close to the median vertical plane of the cavity. At $Ra = 10^6$, the thermal boundary layer on the surface of the lower circular body is accompanied by the formation of a vertical plume at the VC of the cavity.

In the third step, the combined effects of two pairs of circular heating bodies, one placed at the VC of the cavity and the other at the HC of the cavity, are shown in Figure 10(2C). At $Ra = 10^3$ and 10^4, we can see clearly two vortices appearing near the cavity's upper left and right corners and two others are similar with the latter which appear at the lower side (see Fig. 10(2C)). When $Ra = 10^4$, the patterns of the isotherms and the streamlines are generally similar to those when $Ra = 10^3$, because the conduction is significantly dominant. By increasing the Rayleigh number, the role of convection in heat transfer becomes more significant and hence, the buoyancy force, for this reason at $Ra = 10^5$ and 10^6, the intensity of the two vortices which are in the lower part is less than that found in the upper part. At $Ra = 10^6$, the thermal boundary layer becomes more complex at the upper side and thinner around the surface of the circular bodies.

Figure 11 shows the values of $\psi_{\max}$ and $\overline{Nu}_{tot}$ at the same conditions of Figure 10. It is clear that with increasing the Rayleigh number and changing the location of the one pair of circular heating bodies from the HC of the cavity (2A) to the VC (2B), the rate of heat transfer increases. The

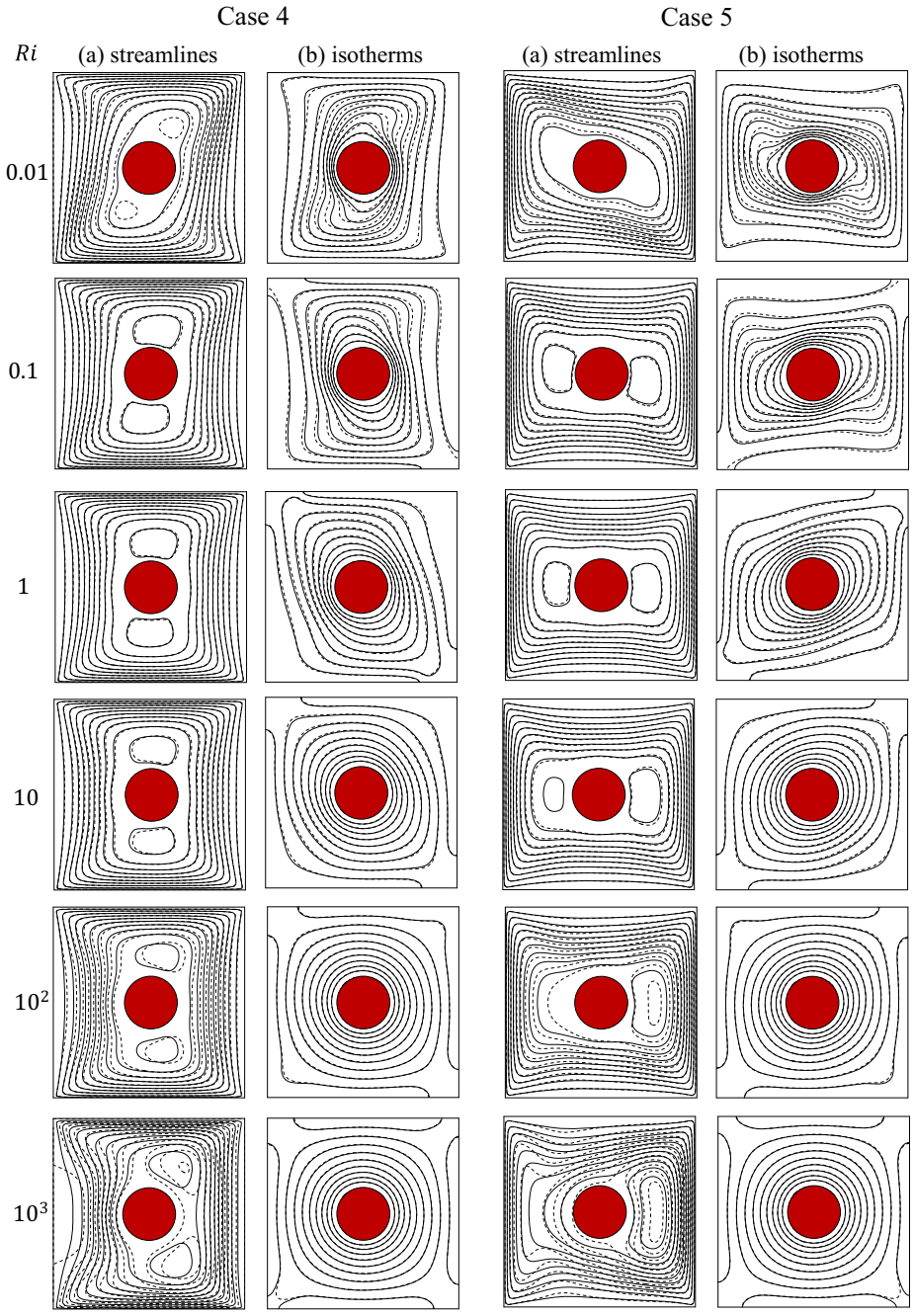

Fig. 14. (a) Streamlines and (b) isotherms inside the cavity with circular heating body ($R = r/H = 0.15$) filled with Cu–water the pure fluid (dashed line) and Cu–water nanofluid (solid line) with $\varphi = 5\%$ and at different Ris for cases 4 and 5 ($Gr = 10^2$).

combined effects (2C) of two pairs of circular heating bodies increase significantly the heat transfer. At high values of the Rayleigh number ($Ra = 10^5$ and 10^6), the optimum value of φ is about 1% in most cases, similar to the previous sections.

5.1.4 Effect of one pair of circular heating and cooling bodies

In this section, results on the effects of one pair of circular heating and cooling bodies on the fluid flow and heat transfer rate are presented considering three different cases (3A, 3B, and 3C) represented in Figure 1 which are explained in three steps.

Figure 12(3A) shows the effects of one pair of circular heating and cooling bodies which is placed at the HC of the cavity, on the streamlines and the isotherms for different Rayleigh numbers, defined in the first step. It can be seen from Figure 12(a) that for $Ra = 10^3$ and 10^4, a counter-clockwise vortex forms inside the cavity between the two circular bodies and four secondary clockwise vortices appear near the cavity corners, the vortices which are in the upper left and lower right corners are more intense than those in the other corners. In Figure 12(b), the uniformly distributed isotherms at this Rayleigh number shows that the main heat transfer mechanism is through conduction.

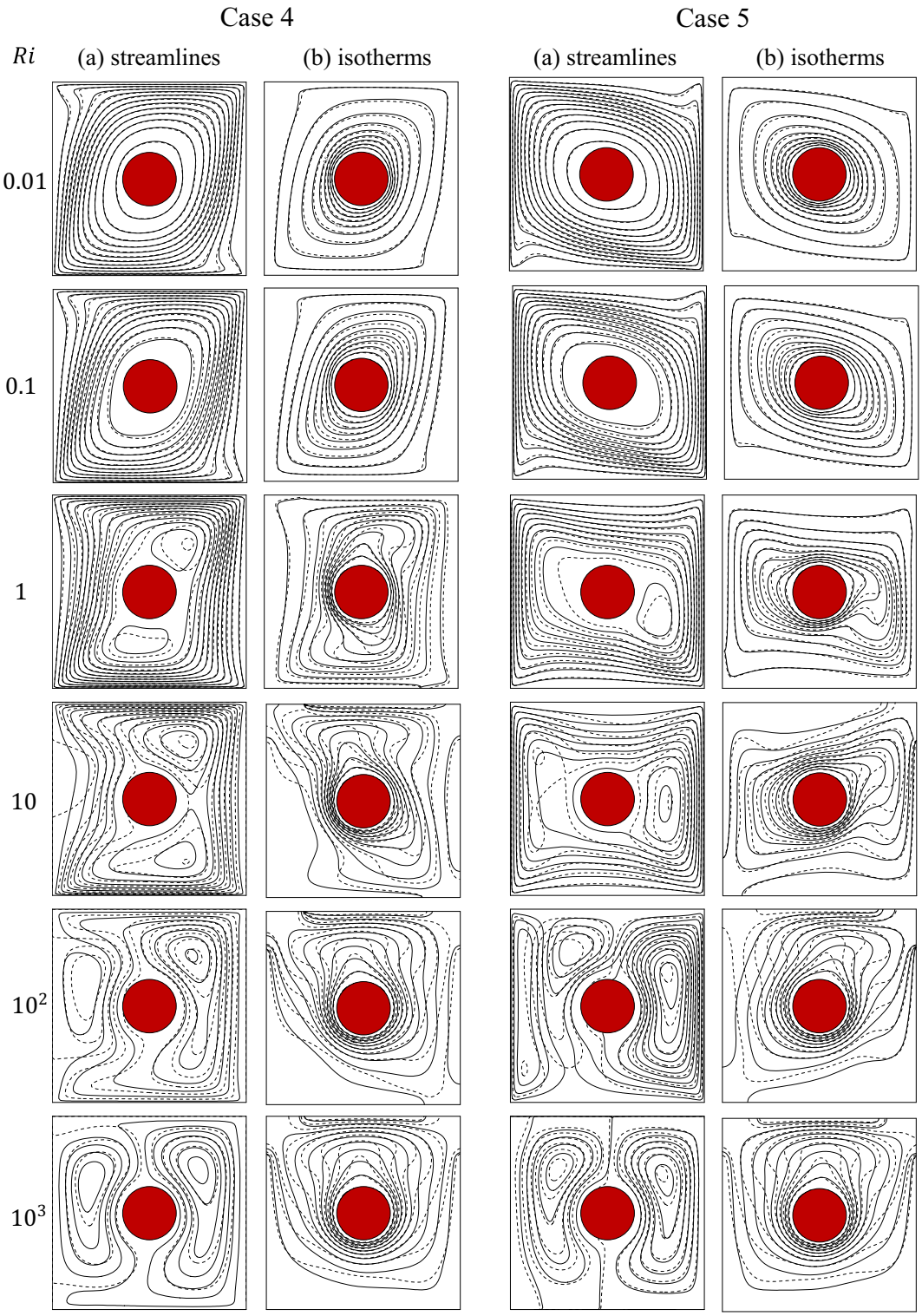

Fig. 15. (a) Streamlines and (b) isotherms inside the cavity with circular heating body ($R = r/H = 0.15$) filled with Cu–water the pure fluid (dashed line) and Cu–water nanofluid (solid line) with $\varphi = 5\%$ and at different Ris for cases 4 and 5 ($Gr = 10^4$).

When $Ra = 10^5$, the intensity of the main vortex increases and becomes with two inner cores and the isotherms get tightened around the circular body (Fig. 12(b)). By increasing Ra beyond 10^5, the path of the fluid particles becomes more and more complex which indicates that the main heat transfer is changing from conduction to the convection mode.

In the second step, the effects of one pair of circular heating and cooling bodies which is placed at the VC of the cavity, on the fluid flow and heat transfer rate are investigated at different Rayleigh numbers. When $Ra = 10^3$ and 10^4, we can see in Figure 12(3B) the rotating eddy with two inner vortices, one on the right side and the other

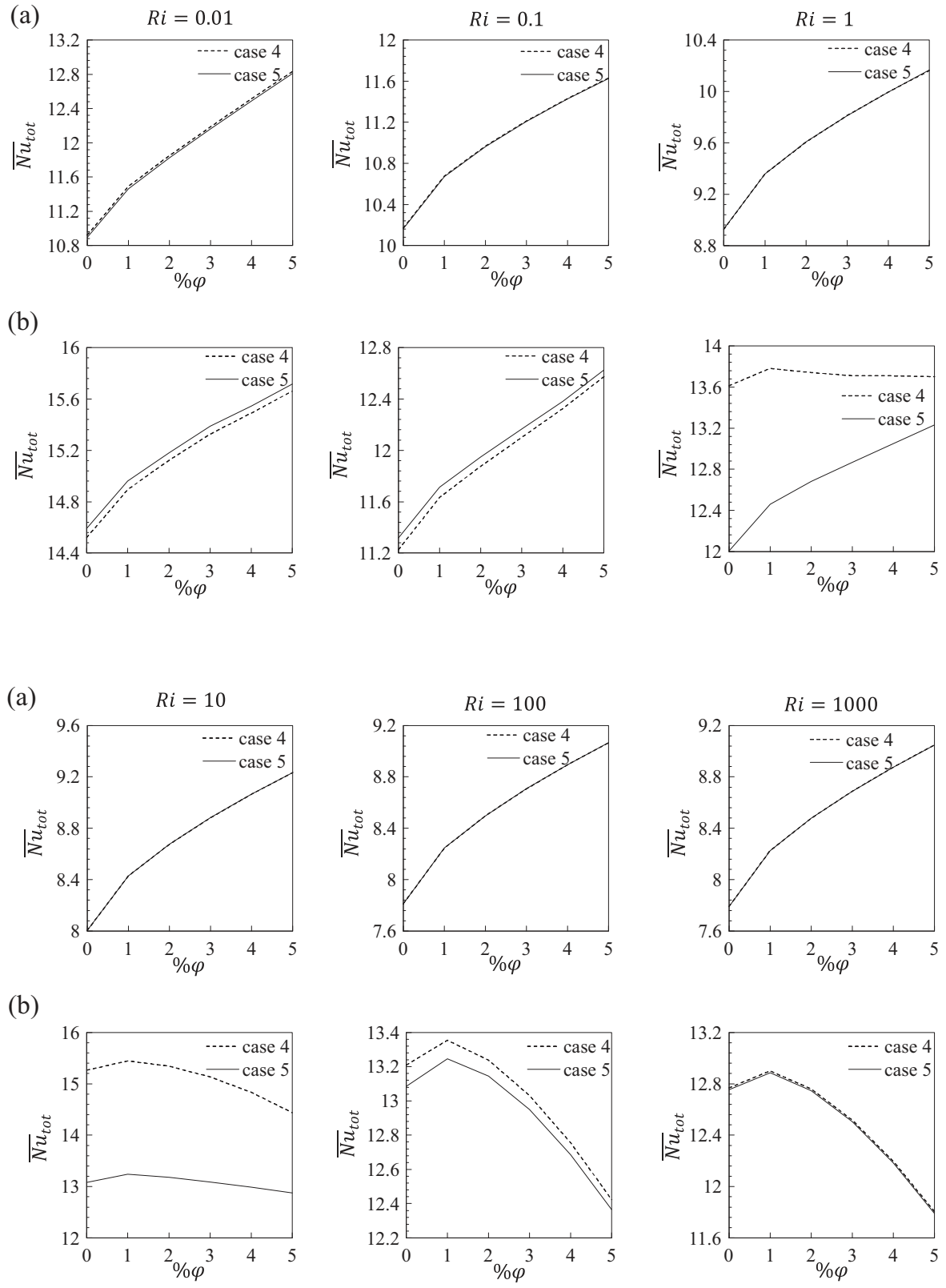

Fig. 16. Variations of $\overline{Nu}_{tot}$ with respect to the volume fraction of the nanoparticles at different Richardson numbers and Grashof numbers for cases 4 and 5. (a) $Gr = 10^2$ and (b) $Gr = 10^4$.

on the left-hand side. By increasing the Rayleigh number, the intensity of the vortices increases and occupies a large space in the cavity. At $Ra = 10^6$, the isotherms are distorted more due to the stronger convection effects, the surfaces of the inner circular body and the cavity become thinner and the thermal gradients on the walls become larger when $Ra = 10^6$, compared to those when $Ra = 10^5$ (see Fig. 12(3B)).

In the third step, the combined effects of two pairs of circular heating and cooling bodies, one placed at the VC of the cavity and the other at the HC are shown in Figure 12 (3C). At $Ra = 10^3$ and 10^4, it can be seen from Figure 12 (3C), four vortices appear near the cavity corners and one between the circular heating and cooling bodies, the vortices which are in the upper right and lower left corners are more intense than those in the other corners of the cavity. By increasing the Rayleigh number beyond 10^5, the intensity of the flow and convection inside the cavity increases and the isotherms become more distorted due to the stranger convection effects.

Figure 13 shows the values of $\psi_{\max}$ and $\overline{Nu}_{tot}$ for the same conditions of Figure 12. At $Ra = 10^3$, we can see clearly that there is no difference between cases (3A) and (3B) in terms of $\overline{Nu}_{tot}$, but by increasing the Rayleigh number, case (3A) becomes better in terms of increasing the heat transfer rate than case (3B) and the combined effects of these two cases (case (3C)) enhance more and more the heat transfer rate. At high values of the Rayleigh number ($Ra = 10^5$ and 10^6), the optimum value of φ is about 1% in most cases but at lower Rayleigh numbers where conduction is dominant, the heat transfer rate is maximum at $\varphi_{opt} = 0.05$.

5.2 MC configuration

In this section, a square cavity with a circular heating body inside, filled with a Cu–water nanofluid is considered for MC heat transfer.

Figures 14 and 15 display the streamlines and isotherms for various values of the Richardson number and the Grashof number. In Figures 14 and 15, case 4 shows the effects of a circular heating body in the cavity with a horizontal moving wall, and case 5 shows the effects of the vertical moving wall. In this configuration, forces due to moving walls of the cavity and the buoyancy act in opposite directions. At small values of the Richardson number ($Ri \leq 0.1$), the flow circulation is mostly generated by the moving walls indicating that the forced convection is dominant. By increasing the Richardson number up to 1, the effects of NC and hence, the buoyancy force becomes stronger and the effects of the moving walls become significantly weakened, then increasing Ri is in favor of NC. The uniformly distributed isotherms at high Richardson numbers for $Gr = 10^2$ shown in Figure 14(b) indicate a conduction-dominated problem and we can note that the isotherms resemble those of NC (see Fig. 3(a)). When $Gr = 10^4$ (Fig. 15(b)), the patterns of the isotherms become more complex which indicates a convection-dominated problem. We can see clearly in Figures 14 and 15 for all Ri values that the difference between the results of a nanofluid and a pure fluid become more evident at higher Richardson numbers ($Ri = 1000$) and this can be explained by the higher viscosity of the nanofluid compared to that of the pure fluid, but at small values of Ri, where forced convection is strongly dominant, the viscosity of the nanofluid does not significantly affect the flow field.

The values of $\overline{Nu}_{tot}$ for cases 4 and 5 are shown in Figure 16 for different Richardson numbers, Grashof numbers and volume fractions of nanoparticles. We can see that by decreasing Ri and increasing Gr, the rate of heat transfer is increased. In addition, at high values of the Richardson number ($Ri \geq 10$) while $Gr = 10^2$ (Fig. 16(a)), the effects of NC are dominant but heat is still mainly conducted. Therefore, the effects of conduction are dominant leading to a maximum heat transfer rate for $\varphi = 0.05$. On the other hand, at $Gr = 10^4$ (Fig. 16(b)) and with a high Richardson number ($Ri \geq 10$), NC dominates. Therefore, the effects of convection are dominant so that the heat transfer rate is maximized for $\varphi \leq 1\%$.

6 Conclusion

This study investigates the role of natural and MC heat transfer of a Cu–water nanofluid in a square cavity with inside circular heating and cooling bodies. The effects of various design parameters such as the location and size are investigated. According to the presented results, the following conclusions are drawn.

6.1 NC configuration

By increasing Ra, the heat transfer rate increases, and at high values of Ra, there is an optimum volume fraction of nanoparticles which maximizes the heat transfer rate and it is about 1% in most cases.

- The results show that when the circular heating body is positioned at the bottom, the heat transfer enhances. The vertical displacement of the circular body has the most important effect on heat transfer rate at high Rayleigh numbers and the horizontal displacement from the VC to the VL of the cavity increases the heat transfer at small Rayleigh numbers.
- By increasing the size of the circular heating body and the Rayleigh number, the heat transfer rate is enhanced.
- By increasing the Rayleigh number and changing the location of the pair of circular heating bodies from the HC of the cavity to the VC, the rate of heat transfer increases. The combined effects of the two pairs of circular heating bodies increase the heat transfer significantly. At high values of the Rayleigh number ($Ra = 10^5$ and 10^6), there is an optimum volume fraction of nanoparticles for which the maximum heat transfer occurs.
- By increasing the Rayleigh number, the pair of circular heating and cooling bodies in the case (3A) becomes better in increasing the heat transfer rate than the case (3B) and the combined effects of these two cases (case (3C)) enhance more and more the heat transfer rate.
- At high values of the Rayleigh number ($Ra = 10^5$ and 10^6), the optimum value of φ is about 1% in most cases but at lower Rayleigh numbers for which conduction is dominant, the heat transfer rate is maximum at $\varphi_{opt} = 0.05$.

6.2 MC configuration

In the case of moving walls at different directions, the heat transfer rate changes significantly, and at high Richardson numbers, the effect of moving walls decreases.

- At small values of the Richardson number ($Ri \leq 0.1$), the flow circulation is mostly generated by the moving walls indicating that the forced convection is dominant.
- The difference between the results of a nanofluid and a pure fluid becomes more evident at higher Ri values.
- By increasing Gr and decreasing Ri, the heat transfer rate increases.
- At high values of the Richardson number ($Ri \geq 10$) while $Gr = 10^2$, the effects of conduction are dominant leading to a maximum heat transfer rate for $\varphi = 0.05$. On the other hand, at $Gr = 10^4$ with a high Richardson number ($Ri \geq 10$), there is an optimum volume fraction of nanoparticles for which the maximum heat transfer occurs.

Nomenclature

C_p	specific heat, $\mathrm{J\,kg^{-1}\,K^{-1}}$
d_p	diameter of the nanoparticle, m
d_f	diameter of the base fluid molecule, m
g	gravitational acceleration, $\mathrm{m\,s^{-2}}$
Gr	Grashof number ($= g\beta\Delta T H^3/\nu^2$)
H	enclosure height, m
k	thermal conductivity, $\mathrm{W\,m^{-1}\,K^{-1}}$
k_b	Boltzmann's constant $= 1.38066 \times 10^{-23}$
$\overline{Nu}_{tot}$	heat transfer of cavity's walls
p	dimensional pressure, $\mathrm{N\,m^{-2}}$
P	dimensionless pressure
Pr	Prandtl number ($= \nu_f/\alpha_f$)
r	radius of circular body
R	non-dimensional radius of circular body ($= r/H$)
Ra	Rayleigh number ($= g\beta_f(T_h - T_c)H^3/\alpha_f\nu_f$)
Re_B	Brownian-motion Reynolds number
Re	Reynolds number ($= U_0 H/\nu$)
Ri	Richardson number ($= Gr/Re^2$)
T	temperature, K
t	time, s
τ	dimensionless time ($t/H/U_{ref}$)
u, v	velocity components, $\mathrm{m\,s^{-1}}$
u_B	Brownian velocity of the nanoparticle, $\mathrm{m\,s^{-1}}$
U, V	dimensionless velocity components
x, y	Cartesian coordinates, m
X, Y	dimensionless Cartesian coordinates (x, y)/H

Greek symbols

α	thermal diffusivity, $\mathrm{m^2\,s^{-1}}$
β	thermal expansion coefficient, $\mathrm{K^{-1}}$
θ	dimensionless temperature
μ	dynamic viscosity, $\mathrm{kg\,m^{-1}\,s^{-1}}$
ν	kinematic viscosity, $\mathrm{m^2\,s^{-1}}$
ρ	density, $\mathrm{kg\,m^{-3}}$
φ	volume fraction of the nanoparticles
ψ	stream function $\left(= -\int_{Y_o}^{Y} U\partial Y + \psi(X, Y_0)\right)$

Subscripts

c	cold
f	fluid
h	hot
nf	nanofluid
s	solid nanoparticles

References

[1] Y.G. Park, M.Y. Ha, H.S. Yoon, Study on natural convection in a cold square enclosure with a pair of hot horizontal cylinders positioned at different vertical locations, Int. J. Heat Mass Transf. 65 (2013) 696–712

[2] F. Garoosi, G. Bagheri, F. Talebi, Numerical simulation of natural convection of nanofluids in a square cavity with several pairs of heaters and coolers (HACs) inside, Int. J. Heat Mass Transf. 67 (2013) 362–376

[3] H.N. Dixit, V. Babu, Simulation of high Rayleigh number natural convection in a square cavity using the lattice Boltzmann method, Int. J. Heat Mass Transf. 49 (2006) 727–739

[4] C.J. Ho, W. Chang, C. Wang, Natural convection between two horizontal cylinders in an adiabatic circular enclosure, J. Heat Transf. 115 (1993) 158–165

[5] C.J. Ho, Y.T. Cheng, C.C. Wang, Natural convection between two horizontal cylinders inside a circular enclosure subjected to external convection, Int. J. Heat Fluid Flow 15 (1994) 299–306

[6] M. Corcione, Heat transfer features of buoyancy-driven nanofluids inside rectangular enclosures differentially heated at the sidewalls, Int. J. Therm. Sci. 49 (2010) 1536–1546

[7] M. El Abdallaoui, M. Hasnaoui, A. Amahmid, Numerical simulation of natural convection between a decentered triangular heating cylinder and a square outer cylinder filled with a pure fluid or a nanofluid using the lattice Boltzmann method, Powder Technol. 277 (2015) 193–205

[8] K. Khanafer, S.M. Aithal, Laminar mixed convection flow and heat transfer characteristics in a lid driven cavity with a circular cylinder, Int. J. Heat Mass Transf. 66 (2013) 200–209

[9] A.W. Islam, M.A.R. Sharif, E.S. Carlson, Mixed convection in a lid driven square cavity with an isothermally heated square blockage inside, Int. J. Heat Mass Transf. 55 (2012) 5244–5255

[10] F. Garoosi, S. Garoosi, K. Hooman, Numerical simulation of natural convection and mixed convection of the nanofluid in a square cavity using Buongiorno model, Powder Technol. 268 (2014) 279–292

[11] Q.-H. Deng, Fluid flow and heat transfer characteristics of natural convection in square cavities due to discrete source-sink pairs, Int. J. Heat Mass Transf. 51 (2008) 5949–5957

[12] H.F. Oztop, I. Dagtekin, Mixed convection in two-sided lid-driven differentially heated square cavity, Int. J. Heat Mass Transf. 47 (2004) 1761–1769

[13] F. Talebi, A.H. Mahmoudi, M. Shahi, Numerical study of mixed convection flows in a square lid-driven cavity utilizing nanofluid, Int. Commun. Heat Mass Transf. 37 (2010) 79–90

[14] H.F. Oztop, I. Dagtekin, A. Bahloul, Comparison of position of a heated thin plate located in a cavity for natural convection, Int. Commun. Heat Mass Transf. 31 (2004) 121–132

[15] M. El Abdallaoui, M. Hasnaoui, A. Amahmid, Lattice-Boltzmann modeling of natural convection between a square outer cylinder and an inner isosceles triangular heating body, Numer. Heat Transf. A 66 (2014) 1076–1096

[16] M. Kalteh, K. Javaherdeh, T. Azarbarzin, Numerical solution of nanofluid mixed convection heat transfer in a lid-driven square cavity with a triangular heat source, Powder Technol. 253 (2014) 780–788

[17] Z. Boulahia, A. Wakif, R. Sehaqui, Numerical study of mixed convection of the nanofluids in two-sided lid-driven square cavity with a pair of triangular heating cylinders, J. Eng. 2016 (2016) 8, Article ID 8962091

[18] Z. Boulahia, A. Wakif, R. Sehaqui, Natural convection heat transfer of the nanofluids in a square enclosure with an inside cold obstacle, Int. J. Innov. Sci. Res. 21 (2016) 367–375

[19] Z. Boulahia, R. Sehaqui, Numerical simulation of natural convection of nanofluid in a square cavity including a square heater, Int. J. Sci. Res. 4 (2015) 1718–1722. ijsr.net

[20] Z. Boulahia, A. Wakif, R. Sehaqui, Numerical investigation of mixed convection heat transfer of nanofluid in a lid driven square cavity with three triangular heating blocks, Int. J. Comput. Appl. 143 (2016) 37–45

[21] Z. Boulahia, A. Wakif, R. Sehaqui, Mixed convection heat transfer of Cu-water nanofluid in a lid driven square cavity with several heated triangular cylinders, Int. J. Innov. Appl. Stud. 17 (2016) 82–89

[22] A. AlAmiri, K. Khanafer, I. Pop, Buoyancy-induced flow and heat transfer in a partially divided square enclosure, Int. J. Heat Mass Transf. 52 (2009) 3818–3828

[23] H.C. Brinkman, The viscosity of concentrated suspensions and solutions, J. Chem. Phys. 20 (1952) 571

[24] J. Maxwell, A treatise on electricity and magnetism, vol. II, Oxford University Press, Cambridge, 1881

[25] M. Corcione, Empirical correlating equations for predicting the effective thermal conductivity and dynamic viscosity of nanofluids, Energy Convers. Manag. 52 (2011) 789–793

[26] A.J. Chamkha, E. Abu-Nada, Mixed convection flow in single- and double-lid driven square cavities filled with water-Al_2O_3 nanofluid: effect of viscosity models, Eur. J. Mech. − B/Fluids 36 (2012) 82–96

[27] R.S. Vajjha, D.K. Das, Experimental determination of thermal conductivity of three nanofluids and development of new correlations, Int. J. Heat Mass Transf. 52 (2009) 4675–4682

[28] A.T. Utomo, H. Poth, P.T. Robbins, A.W. Pacek, Experimental and theoretical studies of thermal conductivity, viscosity and heat transfer coefficient of titania and alumina nanofluids, Int. J. Heat Mass Transf. 55 (2012) 7772–7781

[29] Z. Haddad, H.F. Oztop, E. Abu-Nada, A. Mataoui, A review on natural convective heat transfer of nanofluids, Renew. Sustain. Energy Rev. 16 (2012) 5363–5378

[30] S.V. Patankar, Numerical heat transfer and fluid flow, McGraw-Hill, Washington, 1980

[31] D.B. Spalding, A novel finite difference formulation for differential expressions involving both first and second derivatives, Int. J. Numer. Methods Eng. 4 (1972) 551–559

[32] G. De Vahl Davis, Natural convection of air in a square cavity: a bench mark numerical solution, Int. J. Numer. Methods Fluids 3 (1983) 249–264

[33] G. Barakos, E. Mitsoulis, Natural convection flow in a square cavity revisited: laminar and turbulent models with wall functions, Int. J. Numer. Methods Fluids 18 (1994) 695–719

[34] F.P. Incropera, D.P. DeWitt, Introduction to heat transfer, Wiley, New York, 2002

Cite this article as: Z. Boulahia, A. Wakif, A.J. Chamkha, R. Sehaqui, Numerical study of natural and mixed convection in a square cavity filled by a Cu–water nanofluid with circular heating and cooling cylinders, Mechanics & Industry **18**, 502 (2017)